Hybrid Z-Scheme Using Photosystem I and $BiVO_4$ for Hydrogen Production

*Younghye Kim, Della Shin, Woo Je Chang, Hae Lin Jang, Chan Woo Lee, Hye-Eun Lee, and Ki Tae Nam**

The so-called Z-scheme is a means of utilizing photo-induced electrons from a photosystem and has consistently motivated the design of synthetic photocatalytic systems. Although progress has been made in many pioneering studies on an inorganic-based Z-scheme, there have been no reports of a hybrid Z-scheme for an inorganic and a photosystem. Here, a hybrid Z-scheme is demonstrated by integrating a platinized photosystem I (PSI) and $BiVO_4$ for hydrogen production. Up to now, PSI-driven systems have been limited to a one-step photoreduction reaction using sacrificial reductants. In this hybrid Z-scheme, step-wise charge separation in PSI and $BiVO_4$ enables the production of hydrogen from only water under visible light. PSI and $BiVO_4$ are conjugated via metal mediators to form an all-linked structure. The novel design exhibits potential for the development of a protein hybrid system for electrochemical devices, sensors, and a solar energy conversion system.

1. Introduction

In natural photosynthesis, the two-step photo-induced charge separation in photosystem II (PSII) and photosystem I (PSI) and an electron chain between the two photosystems follows a Z-scheme. First, a hole is generated from the charge separation step in PSII that oxidizes two water molecules into an oxygen and four protons, and the excited electron moves to PSI through the electron transport chain. The electron is finally excited in PSI and gains sufficient potential energy (–0.58 V vs NHE, pH 7) to reduce nicotinamide adenine dinucleotide phosphate ($NADP^+$).[1] The stepwise charge transfer reaction provides the efficient light-to-chemical energy conversion from only water and visible light (**Scheme 1**a). Generally, approximately 28.2% of the total sunlight is converted into chemical energy as adenosine triphosphate (ATP) and reduced nicotinamide adenine dinucleotide phosphate (NADPH) in the light reaction of natural photosynthesis.[2]

Y. Kim, D. Shin, Dr. H. L. Jang, C. W. Lee, H.-E. Lee, Prof. K. T. Nam
Department of Materials Science and Engineering
Seoul National University
Seoul 151-744, Korea
E-mail: nkitae@snu.ac.kr
W. J. Chang, Prof. K. T. Nam
Interdisciplinary Program for Bioengineering
Seoul National University
Seoul 151-742, Korea

DOI: 10.1002/adfm.201404556

This natural Z-scheme has inspired an artificial Z-scheme, which has been used in photocatalytic fuel production. In recent years, hydrogen fuel production from nonsacrificial water splitting has been studied by combining half-reactions that produce H_2 and O_2. In 1979, Bard introduced photosynthesis as a model system for water splitting using dual semiconductors.[3] This novel approach enabled H_2 production from water using only visible light. Numerous studies on material development and system design have since been conducted to exploit solar light to the greatest extent possible. Generally, metal oxides,[4–6] metal (oxy)nitrides,[7,8] and metal sulfides[9] have been utilized as charge separating photocatalysts, and proper cocatalysts have been loaded to catalyze H_2 and O_2 production.[10] For H_2 evolving part, Pt[7], Ru,[4,11] and Ni-based[9] cocatalysts have been studied to enhance the photocatalytic activity. To obtain an optimal band position, some photocatalysts were further engineered with dopants[12] or treated to form solid solutions.[13]

Another interesting approach to modeling natural photosynthesis is a direct utilization of photosystems for a H_2-evolving photocatalyst. PSI is a naturally existing photocatalyst that possesses solar light-active chlorophyll dyes that have an optimal structure for efficient energy transfer. The P700 reaction center at the center of PSI has a charge separation efficiency near unity and a low excitation energy of 1.77 eV (λ = 700 nm).[1] Therefore, PSI itself is very attractive photocatalyst that can be used in natural environments. Recently, PSI hybrid systems have been fabricated by conjugating artificial or biological cocatalysts. Generally, PSI has been platinized to deposit platinum nanoclusters on the electron emitting stromal side of a protein by the photoreductive deposition reaction, $[PtCl_6]^{2-} + 4e^- + h\nu \rightarrow Pt + 6Cl^-$.[14–16] Similarly, a cocatalyst has been conjugated using a chemical linker. Recently, Pt or Au nanoparticles[17] and hydrogenases[18] have been covalently linked to PSI to dramatically enhance its H_2 evolution activity. However, to position a chemical linker at the desired position, PSI was reconstituted mostly by engineering cysteine (Cys) residues for use in dithiol molecular wire. The most recent studies have reported the self-assembly of molecular catalysts, such as a Ni catalyst[19] and cobaloxime.[20] However, all of these PSI hybrid systems only mimic the one-step photoreduction in PSI, which requires that a chemical donor, such as ascorbic acid, be mixed into the reaction solution. In this study, we implemented a full

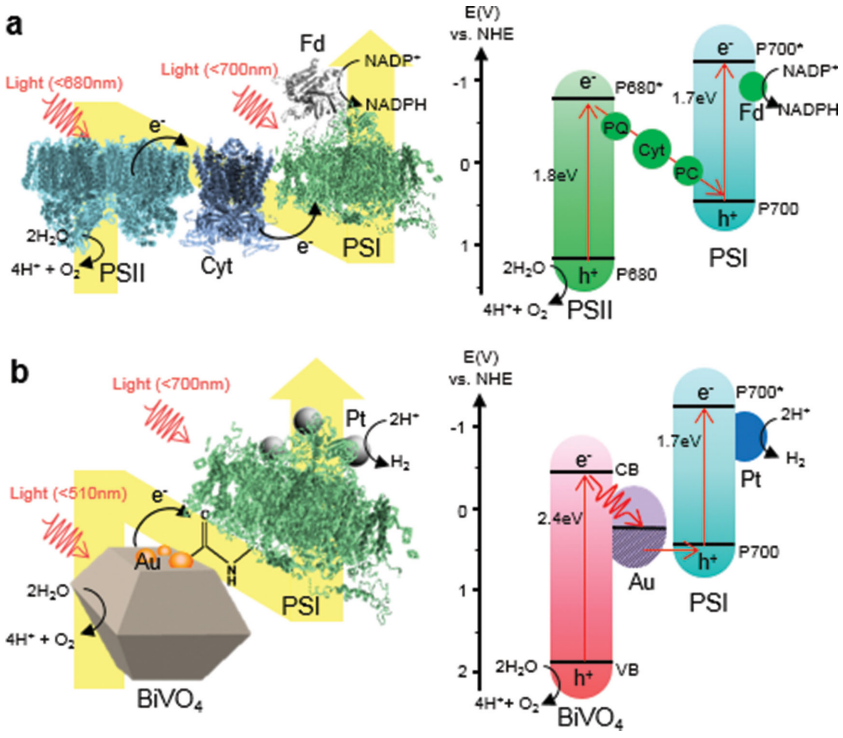

Scheme 1. a) Natural Z-scheme and its energy diagram; photosynthesis follows serial reactions: oxidation of water and electron excitation in PSII, electron transfer through electron transport chain (plastoquinone (PQ), cytochrome c6 (cyt), plastocyanin (PC)), electron excitation in PSI, and reduction of NADP in ferredoxin-$NADP^+$ reductase (FNR). b) Our hybrid Z-scheme and its energy diagram (mediator is Au). Photosynthetic water splitting follows serial reactions: oxidation of water and electron excitation in $BiVO_4$, electron transfer through Au, electron excitation in PSI, and reduction of hydrogen catalyzed by Pt.

Z-scheme for the H_2 evolution from water using platinized PSI (PtPSI) and synthesized semiconductor. The semiconductor particle replaced the role of PSII, serving both as a photocatalyst for water oxidation and an electron supply for PSI. This is the first report of the use of a protein-photocatalyst system for H_2 production from water without the use of an additional reducing additive, which we call a "hybrid Z-scheme".

Two types of structural design are generally used in a Z-scheme, depending on the mediating role between the two reaction centers. First, when the electron mediator is a redox couple in the form of ion pairs, the two reaction centers are physically separated. However, the redox pair can induce an undesirable back reaction and dissipate the electrons and holes that participate in the intended pathway. Moreover, it is often difficult to operate a redox couple-mediated system over a wide pH range.[21] In the second design, a conducting material can be employed as a mediator to transfer electrons directly between the reaction centers. The two reaction centers are thus physically linked via a conductor to form an "all-solid-state". The integration of two reaction centers with a conductor between the centers creates an ohmic contact and reduces the distance for electron transfer. Thus, the back reaction is prevented, and the working conditions are expanded to a wide pH range and even to the gas-phase.[21] Recently, a reduced graphene oxide was used as a solid electron mediator for all-solid-state water splitting using $BiVO_4$ and $Ru/SrTiO_3$:Rh photocatalysts,[11] and innovative developments in H_2-evolution systems have been realized by designing various all-solid-state Z-schemes using conducting mediators.[12,22] Our hybrid Z-scheme was also constructed in an all-solid-state by attaching metal particles onto a semiconductor to form a chemical linker between the metal and PSI. The metal-deposited semiconductor served both as a stable support and a direct electron supplier for PSI. In a natural thylakoid membrane, photosynthetic proteins are stably inserted into the lipid membrane, resulting in a fluid structure where the proteins are arranged in a fixed position and orientation. Immobilizing a PSI on the metal should be analogous to inserting a PSI in the thylakoid membrane. In this study, we compared with linked system and an unlinked but mixed system and analyzed the positive effects of the all-linked system.

In the designed system, $BiVO_4$ was selected as the semiconductor component. $BiVO_4$ has both a suitable valence band for water oxidation (2.75 V vs NHE) and a low bandgap for visible light absorption (2.43 eV).[23] Gold (Au) or silver (Ag) nanoparticles were deposited on the surface. The work functions of these nanoparticles (–5.1 eV for Au and –4.7 eV for Ag)[24] are both located between the conduction band of $BiVO_4$ and the redox potential of the PSI reaction center (P700, 0.47 V vs NHE, pH 8),[25] such that these nanoparticles can serve as a conducting mediator between two components. Scheme 1b shows the structural model and the energy diagram of the hybrid Z-scheme with an Au mediator. In terms of its light absorption properties, the PSI harvests solar light through chlorophylls that efficiently absorb red (≈700 nm) and blue (≈450 nm) light, and $BiVO_4$ absorbs light with wavelengths below 510 nm. Therefore, the absorption range in the hybrid Z-scheme encompasses the entire visible light range. Metal particles were carboxyl-functionalized for covalently conjugation with PtPSI via EDC/Sulfo-NHS coupling. The metal-deposited $BiVO_4$ (mt-$BiVO_4$) and PtPSI constituted a hybrid Z-scheme in an all-solid-state form, which successfully evolved H_2 from water under visible light.

2.1. Synthesis of Hybrid Z-Scheme

2.1.1. Platinization of PSI

PSI was extracted from spinach and characterized by SDS-PAGE. The isolated thylakoid membrane fragments were distributed into three layers via a sucrose density gradient (**Figure 1**a). The thick upper layer consisted of a light harvesting complex II (LHCII) and other protein fragments, and the middle and lower layers consisted of monomeric and aggregated PSI, respectively. Each protein layer was injected using a syringe and analyzed by SDS-PAGE (Figure 1b).

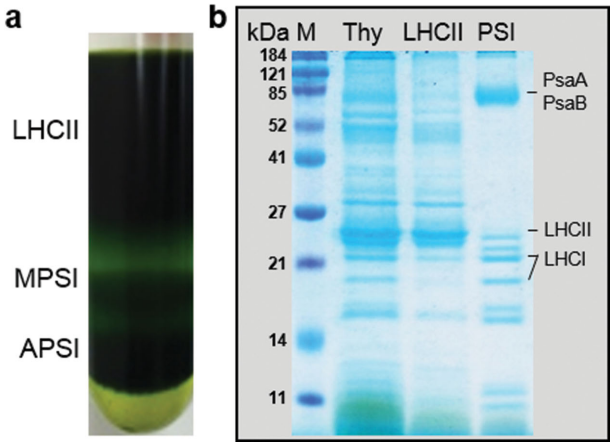

Figure 1. a) Sucrose density gradient resulting in three separate layers: LHCII-rich thylakoid, monomer PSI (MPSI), and aggregated PSI (APSI); b) SDS-PAGE of thylakoid before ultracentrifugation (Thy), LHCII-rich thylakoid fragment (LHCII, upper layer in (a), and PSI (PSI, middle, and bottom layer in (a). Identified main bands are marked with the name of component.

PSI was identified by a significant band that was assigned to PsaA and PsaB polypeptides and other minor polypeptide bands that are not marked in the figure.[26] Two bands also appeared that corresponded to the light harvesting complex I (LHCI). In a plant thylakoid, the LHCI surrounds a PSI core to collect light and transfer the photoenergy to the PSI core. Previous studies on bacterial photosynthetic proteins have demonstrated that a light harvesting antenna-reaction center core complex exhibits higher photoactivity than a bare reaction center core in vitro.[27] Thus, we expected LHCI to serve as an extra light collector in our LHCI-PSI complex and used as this form for the remaining procedures. The polypeptides from the PSI bands virtually disappeared in the LHCII-rich band, which showed that PSI was well-isolated from the thylakoid membrane.

The H_2 evolution efficiency of the PtPSI was measured by gas chromatography before the PtPSI was linked to the $BiVO_4$-metal complex. During the 20 h of the photoreduction process, ≃1 μmol H_2 mg Chl^{-1} of H_2 was generated. Detectable H_2 (< ≃0.01 μmol H_2 mg Chl^{-1}) was produced after 6 h, which corresponded to the platinization stage of PSI. After the initial platinization stage, the H_2 production rate increased dramatically. The maximum activity was reasonable compared with previous reports for platinized PSI systems, as shown in **Table 1**. Typically, PSI extracted from thermophilic bacteria exhibits higher photoactivity and stability. However, we used spinach as a source material to simplify the extraction method and mass produce the final protein.

2.1.2. Photodeposition of Metal Nanoparticles on $BiVO_4$

To selectively extract electrons, single crystal monoclinic $BiVO_4$ was synthesized by a hydrothermal method. The synthesized particles were then characterized by XRD (**Figure 2**a) and field emission scanning electron microscopy (FESEM) (Figure 2b). The XRD pattern was well-matched with that of monoclinic $BiVO_4$, which corresponds to the standard card No. 14–0688. The decahedral shape and fine crystallinity of $BiVO_4$ was observed in the FESEM images. The two square exposed facets corresponded to the {010} facet, which was the electron-accumulated facet, and the isosceles trapezoidal facets at the other sides corresponded to the {110} facet, which was the hole-accumulated facet.[28] Thus, the Au and Ag particles were selectively deposited on the {010} facet of $BiVO_4$ by accepting electrons on the surface.

The photodeposition of Au and Ag was carried out using $HAuCl_4$ and $AgNO_3$ metal precursors in water, respectively, which functioned as hole scavengers. A large number of small-sized metal particles can be used to extend the contact surface between the materials and reduce the electron migration distance. In the experimental process, the initial precursor concentration was optimized to 10 wt%, because a further increase in the precursor did not significantly improve the deposited area. The number of deposited particles saturated in ≃3 h, and further reaction only enlarged the particle size.

The mt-$BiVO_4$ particles that were synthesized by the optimized procedure were observed using FESEM (Figure 2c,d). The diameters of both the Au and Ag particles were distributed between 100 and 200 nm, which was approximately sevenfold larger than the size of the monomeric PSI. We integrated the area of the exposed {010} facet and the metal-deposited partial area using the FESEM images. The resulting average ratio of the area of the metal-deposited surface to that of the {010} facet was approximately 11% for Au–$BiVO_4$ and 30% for Ag–$BiVO_4$. Assuming that the area of {010} facet of a $BiVO_4$ particle was 10 μm^2 and that PSI was densely bound to the flat metal surface as monolayer, 6 400 (for the Au-deposited particles) and 17 000 (for the Ag-deposited particles) monomeric PSI should have been conjugated to a single $BiVO_4$ particle. Conversion to the macroscopic scale showed that 0.016 mg Chl (for the Au-deposited particles) and 0.043 mg Chl (for the Ag-deposited particles) of PSI were the equivalent binding amounts for 1 g of $BiVO_4$.

2.1.3. Optical Property Analysis

The optical properties of the two photocatalysts were investigated by UV–visabsorption. The absorption spectra were

Table 1. H_2 evolution activity in PtPSI. The extracted PSIs are all wild type and are not rebuilt.

Year	Source of PSI	Electron donor, mediator	Maximum activity [μmol H_2 h^{-1} mg Chl^{-1}]	Light source
This study	Spinach	Asc, Dc	0.08	White LED
(2001)[15]	Spinach	Asc, PC	2	LED (660 nm)
(2004)[16]	Spinach	Asc, Corss-linked PC	0.09 (0.03 without PC)	150-W halogen lamp (<600 nm)
(2010)[14]	Thermophilic bacteria	Asc, Cyt	5.5	150-W halogen lamp (<590 nm)

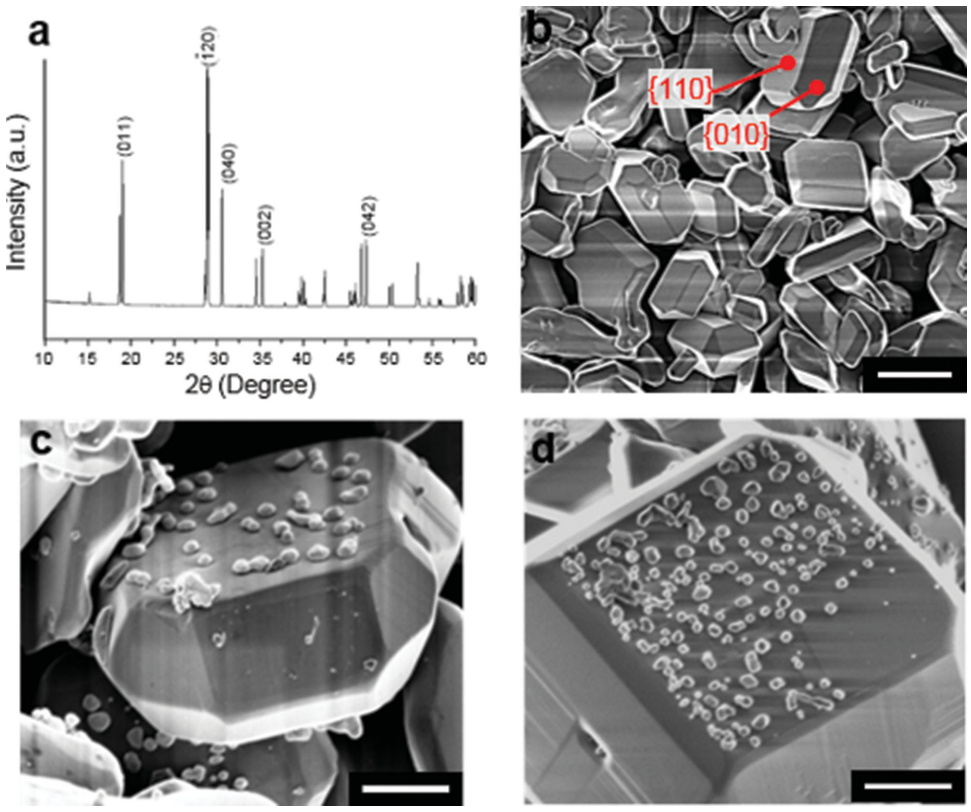

Figure 2. a) XRD pattern of monoclinic $BiVO_4$ (JCPD #14–0688); b) FESEM image of $BiVO_4$; c) Au–$BiVO_4$; and d) Ag–$BiVO_4$. Scale bar: 4 μm for (b) and 1 μm for (c,d).

recorded for isolated PSI (which is shown as a green solid line in **Figure 3**), which exhibited two primary peaks at 436 and 678 nm. The minor peak at 471 nm that was observed in the spectra corresponded to the light harvesting complex I (LHCI) that surrounded the PSI core.[26] The diffuse reflectance of $BiVO_4$ was measured, and the spectra is presented as a blue dotted line in Figure 3. Our $BiVO_4$ absorbed light effectively below 510 nm.

In this study, we used a white light emitting diode (LED) bulb, which is a commonly used indoor light, as a light source to provide the full spectrum of visible light with an intensity near the light saturation point of PSI (190 μE m^{-2} s^{-1} with a 660 nm LED).[15] Our light source had an intensity of 186 μE m^{-2} s^{-1} between 650 and 700 nm and of 91 μE m^{-2} s^{-1} below 510 nm. The mild intensity of the light source prevented a temperature rise in the reactor and unnecessary energy dissipation. Figure 3 shows the irradiance intensity spectra for different wavelengths, which are fitted with a black line.

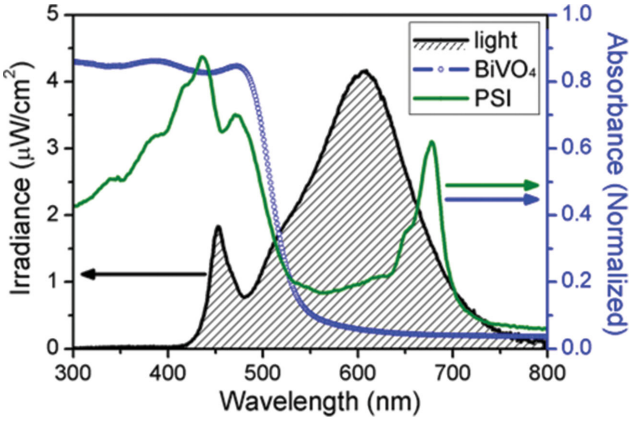

Figure 3. Absorption spectra of PSI (green line) and $BiVO_4$ (line with blue circle) and irradiance spectra of LED light used in this study (black line).

2.1.4. Hybridization of PtPSI and mt-$BiVO_4$

The as-prepared PtPSI and mt-$BiVO_4$ was integrated into the hybrid system. To carboxylate the metal surface, the synthesized mt-$BiVO_4$ was treated with an MPA ethanolic solution. An amide bond was then formed between the carboxyl group on the metal and the amine group on PSI by EDC/Sulfo-NHS coupling. Generally, the primary amine in the lysine (Lys) residue has the highest activity; thus, most of the amide bond was expected to be formed on the Lys of the protein surface. The Lys was densely located on both the lumen and stromal side of PSI, which are shown as magenta spheres in **Scheme 2**. In platinization, the reduction of Pt occurred primarily at the stromal side of the electron emitting site, such that the Pt nanoclusters were expected to cover the electron emitting site of PSI (which is shown as orange spheres in Scheme 2). Therefore, some of the exposed active residues in stromal side may have been blocked. However, the active residues on the lumen side were exposed

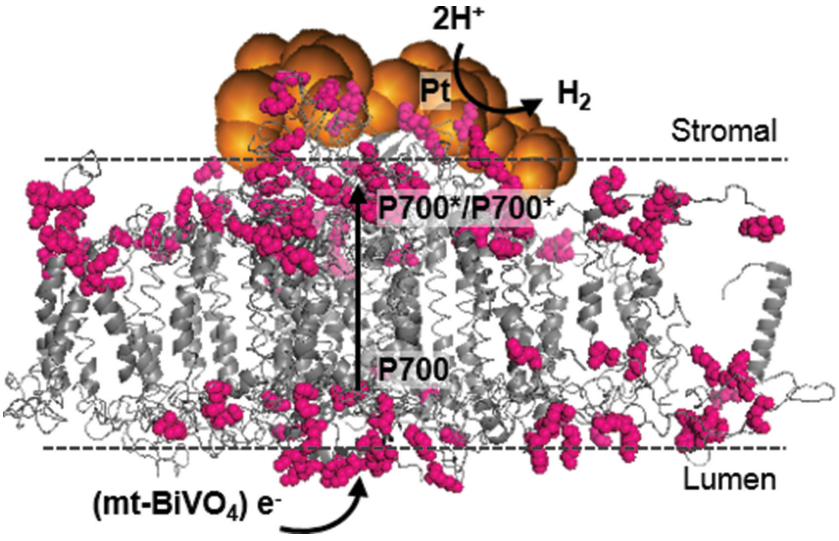

Scheme 2. Molecular structure of PtPSI showing emphasized Lys, which are the primary targets in EDC/sulfoNHS coupling. Pt nanoclusters and Lys are shown as orange and magenta spheres. The electron pathway from lumen side to stromal side is shown with arrows (PDB entry 2WSC).

without obstruction and could freely form an amide bond. The amide bond at the lumen side provided a favorable pathway for the acceptance of electrons from mt-$BiVO_4$.

As mt-$BiVO_4$ is a microparticle, it sinks into a solution within a few minutes (see Au–B and Ag–B in **Figure 4**b). However, after coupling to the PtPSI, some of the particles were still dispersed in solution after 1 h holding time (see Au-B-PtPSI and Ag-B-PtPSI in Figure 4b). The upper greenish section contained both unlinked PtPSI and all-linked particles. The absorption spectra of the upper dispersed particles were removed for the absorption measurements. In Figure 4a, the broad absorption spectra over the entire wavelength range corresponded to the $BiVO_4$ particles that were dispersed in solution, and the observable peaks at the wavelengths of red and blue light corresponded to the PtPSI. To calculate the amount of the linked PtPSI, the micro-particles were removed by gentle centrifugation, and the concentration of the remaining PtPSI particles was measured from the absorbance spectra. Thus, 0.08 ± 0.03 and 0.16 ± 0.05 mg Chl of the PtPSI decreased in the solution after coupling with 1 g of Au–$BiVO_4$ and Ag–$BiVO_4$, respectively. The differing amounts that were bound on Au and Ag resulted primarily from the different deposited areas of the metal particles.

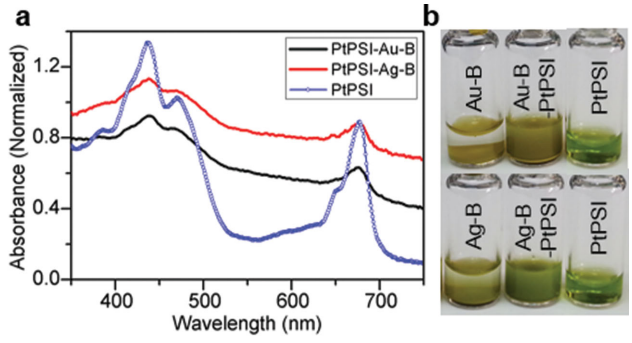

Figure 4. a) Absorption spectra of PtPSI (line with blue circle), dispersed PtPSI linked with Au–$BiVO_4$ (red) and Ag–$BiVO_4$ (black); b) image of synthesized samples after 1 h holding time at room temperature. B denotes $BiVO_4$.

2.2. Electron Transfer Study in the Hybrid System by PL Analysis

We evaluated the electron motion in the hybrid system by PL analysis (**Figure 5**). The PL spectra were observed for four different samples, $BiVO_4$, mt-$BiVO_4$, mt-$BiVO_4$ with PtPSI, which was simply mixed together (Mixed) and covalently all-linked by EDC coupling (Linked). In monoclinic $BiVO_4$, UV excitation generates holes in the O_{2p} band, and the electrons in the V_{3d} band and the excitation energy can be relaxed by recombination at Bi_{6s}.[29] Our $BiVO_4$ exhibited a PL peak at approximately 540 nm in agreement with previous reports.[30] We first observed the PL quenching effect by metal deposition. The metal particle covering the electron emitting facet can accept electrons from the V_{3d} conduction band of $BiVO_4$ and decreases recombination. The PL intensity at 540 nm for Au–$BiVO_4$ (Figure 5a,b) and Ag–$BiVO_4$ (Figure 5c,d) was 93% and 62% of that of pure $BiVO_4$. This result suggests that Ag offers an advantage over Au in electron extraction. Structurally, the deposited area of Ag is approximately threefold that of Au, which can result in more effective quenching. Besides, plasmonic metal can increase or decrease PL in various ways including local electric field enhancement, radiative/nonradiative decay enhancement, and energy quenching inducement. The PL quenching observed in this study may be the result of these coupled effects. In our system, transfer of excited electron to metal and plasmon-driven PL enhancement occurred simultaneously.

To observe additional electron transfer to the protein, the mt-$BiVO_4$ was combined with the PtPSI. The use of the protein resulted in electron transfer from the metal to P700 and induced extra quenching. In the analysis, 0.5 µg Chl of the PtPSI was mixed with and linked to 1 mg of the mt-$BiVO_4$ (Figure 5a,b). In both the Au–$BiVO_4$ and Ag–$BiVO_4$, the PL of the covalently linked system was quenched more than that of the simply mixed system. This result supported the hypothesis that chemical bonding between metal and protein facilitated efficient electron transfer from the $BiVO_4$ conduction band to the PSI. The amount of the PtPSI was then reduced to 0.05 µg Chl, which was comparable with the theoretical equivalent binding amount of the PSI on Ag–$BiVO_4$. Herein, the linked system exhibited noticeable quenching, whereas there was nearly negligible quenching in the mixed system (Figure 5b,d). Thus, the quenching effect resulted primarily from only the linked PtPSI. Interestingly, the PL quenching in the linked system with 0.05 µg Chl PtPSI was comparable to that in the mixed system with 0.5 µg Chl of the Pt PSI.

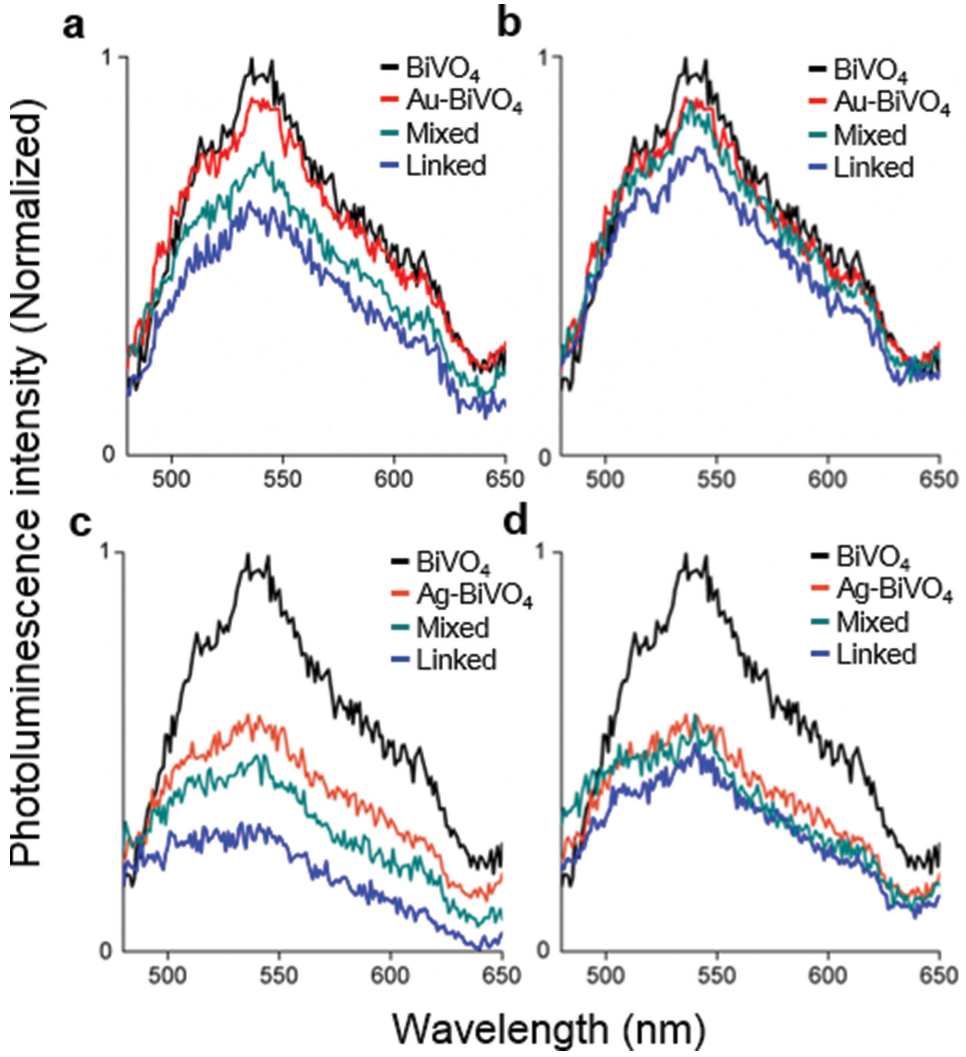

Figure 5. a) PL spectra of Au–$BiVO_4$ with 10 equivalent PtPSI; b) PL spectra of Au–$BiVO_4$ with one equivalent PtPSI; c) PL spectra of Ag–$BiVO_4$ with 10 equivalent PtPSI; d) PL spectra of Ag–$BiVO_4$ with one equivalent PtPSI.

2.3. H_2 Evolution Measurement by GC Analysis

The H_2 evolution rate was measured by GC. The hybrid Z-scheme using Au and Ag mediators exhibited an H_2 evolution activity of 34 and 15 nmol h^{-1}, respectively (**Figure 6**a). To our knowledge, this result is the first observation of H_2 evolution from a protein-photocatalyst system in which only water was used as an electron source. The calculated external quantum efficiency of the system was approximately 10^{-5}. Such a low quantum efficiency resulted primarily from the inefficient hybrid ratio of the reduction component of the PtPSI to the oxidation component, $BiVO_4$. The oxygen evolution activity of monoclinic $BiVO_4$ with a $NaIO_3$ sacrificial agent has been previously reported to be approximately 100 μmol h^{-1} g^{-1}.[31] Considering that four electrons from the oxidation step immediately move to PSI via the metal mediator in the Z-scheme, 400 μmol h^{-1} of electrons can be supplied to PSI from 1 g of $BiVO_4$. However, considering that the maximum amount of the PtPSI was conjugated on $BiVO_4$, the activity of the photoreduction from the equivalently bound protein lagged far behind (at approximately 1/160 000 (for Au-deposited particles) and 1/58 000 (for Ag-deposited particles)) the photo-oxidation in the semiconductor component of the hybrid system. The imbalance between the oxidation and reduction rates was the primary limitation of the hybrid system in terms of the efficiency. To overcome the imbalance in the combination ratio, nanoscale semiconductor particles should be used to increase the surface area for protein binding. The photoreaction proceeded for 72 h, and H_2 was collected every 24 h. Figure 6b shows the measured amount of H_2 from our Z-scheme using Au and Ag mediators. The initial H_2 evolution activity lasted steadily for 72 h and even slightly increased in some cases. In this regard, we expect that the unlinked, but attached PSIs in the vicinity of activated metal formed new amide bonds during the photoreaction, followed by providing additional linked Z-scheme.

When the PtPSI and mt-$BiVO_4$ components were mixed without covalent conjugation to serve as a reference, the H_2 evolution activity was lowered to approximately 1 nmol h^{-1} (Figure 6a). In order to clarify the pathway of H_2 evolution, several mt-$BiVO_4$ samples also have been investigated by GC

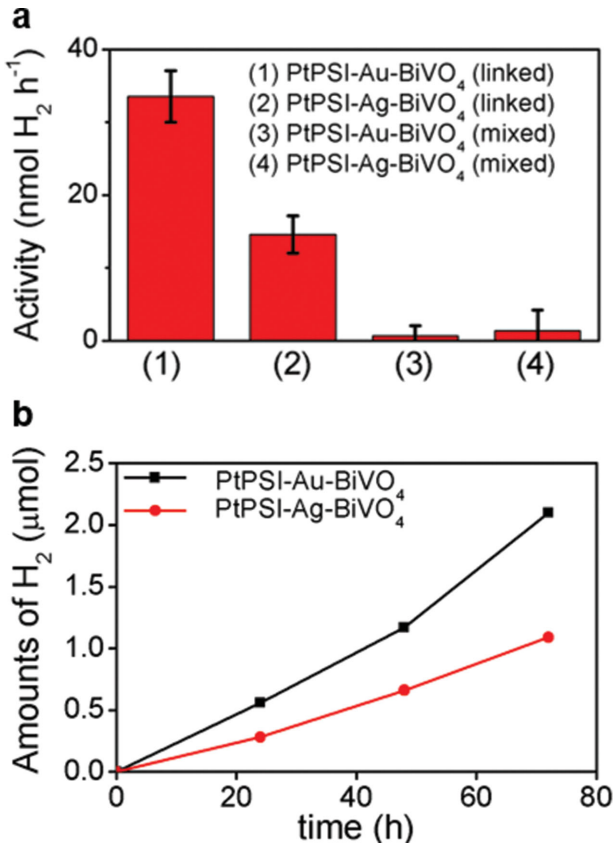

Figure 6. Hydrogen evolution activity measured by GC (for 1 g of sample). a) The average hydrogen evolution activity for 48 h. b) The hydrogen evolution activity as a function of operation time. The produced hydrogen was measured every 24 h from the same sample.

analysis. As a result, all the contrast samples including Au–$BiVO_4$, Ag–$BiVO_4$, Pt–$BiVO_4$, and pure $BiVO_4$ showed no H_2 evolution activity when the deposited metal was either activated with EDC/Sulfo-NHS or inactivated.

When the H_2 evolution activity was recalculated considering the bound PtPSI, 0.42 ± 0.20 and 0.091 ± 0.044 μmol h^{-1} mg Chl^{-1} of H_2 were produced in the Au- and Ag-mediated systems. The activity was much higher (for the Au-deposited particles) or analogous (for the Ag-deposited particles) to the activity that was measured during the platinization step using an Asc/Dc electron donor couple. In platinization, PSI receives an electron from the Asc/Dc reductant couple that is dissolved in solution, whereas PSI in our hybrid Z-scheme received an electron from the directly linked metal. Similarly, in nature, the bound mediator PC, transfers an electron directly to the lumen side of PSI.[32] Thus, we hypothesized that our all-linked system effectively realized an electron transfer chain and exhibited enhanced or comparable activity for PSI relative to the half-reaction system with a chemical electron donor. In addition, we expect that the linker could be designed to significantly enhance the activity even further.

The Au mediator more than doubled the H_2 evolution activity over that of the Ag mediator. Considering the improved quenching of PL in the Ag-mediated Z-scheme over the Au-mediated Z-scheme, it was interesting that the Au mediator showed significantly higher H_2 evolution activity. We hypothesize that the Au provided a moderate metal-to-$BiVO_4$ potential barrier that prevented electron back transfer, whereas the small potential barrier in Ag–$BiVO_4$ could easily have induced the back transfer of electrons. We also expect that a suitable surface plasmon resonance of Au could contribute to enhanced photoactivity.[33] Ag also exhibits a considerable plasmon effect; however, the resonance wavelength of Ag is located at the edge of our light source spectrum.[34] Recently, light absorption enhancement has been demonstrated by the plasmon effect of Ag nanoparticles in an all-solid-state Z-scheme.[35] We expect that the Au nanoparticles in the hybrid Z-scheme could also provide extra absorption and enhance the electron supply to the PSI. In addition, other roles of Au nanoparticle as a hot electron source or a hole scavenger should be considered in order to comprehensively understand the electron mediating pathway through Au nanoparticle.[36]

In this study, we have successfully demonstrated the first hybrid Z-scheme for H_2 evolution. Our hybrid Z-scheme was designed to split water and evolve H_2 as a final product at PtPSI. Thus, we expected that O_2 would evolve on the semiconductor side as a water oxidation product, but we also considered the possibility of the evolution of reactive oxygen species, such as hydroxyl and superoxide anion radicals. These radicals are commonly reported to be detected in metal(oxide)-doped semiconductors in competition with O_2 and H_2.[37] In the current study, we did not perform quantitative measurements of all of the oxygen species from the Z-scheme, and we are currently investigating the use of H_2O^{18} as a reactant to categorize and quantify the direct products. Despite the insufficient analysis of the oxygen reaction products, we were still able to verify the successful operation of the hybrid Z-scheme by measuring the target product, H_2. First, the use of the hybrid Z-scheme was successful in realizing the protein-photocatalyst system for the evolution of water-sacrificed, visible light-driven H_2. Moreover, we demonstrated the effects of a directly linked structure and plasmonic nanoparticle mediators on the activity of the system. Thus, the issues that were explored in this study can open new avenues in the development of other protein hybrid systems for various applications.

3. Conclusion

We developed a hybrid Z-scheme for H_2 evolution by integrating $BiVO_4$ and a PtPSI in an all-solid-state. Under visible light, our system showed the ability to evolve hydrogen from water without the use of additional sacrificial agents or redox mediators for the first time. The water-sacrificed H_2 evolution was a successful demonstration of the utility of a PSI as a photocatalytic material. In designing this structure, we constructed an all-linked hybrid system using Au and Ag nanoparticle conductors. The positive effect of direct linking between a protein and a metal mediator was revealed by effective PL quenching and enhanced H_2 evolution activity. We demonstrated the enhanced activity of PSI over that of a solvent-based sacrificial reaction and found that the plasmon effect of the metal could further amplify the electron supply. This hybrid system provides a new means of using a photosynthetic protein as a

practical material in the design of a photocatalytic energy producing system.

4. Experimental Section

Chemicals: Sodium ascorbate (Asc, 98%), 2,6-dichloroindophenolate hydrate (Dc, 90%), sodium hexachloroplatinate(IV) hexahydrate ($Na_2[PtCl_6]$, 98%), gold(III) chloride trihydrate ($HAuCl_4{\cdot}3H_2O$, 99.9%), silver nitrate ($AgNO_3$, 99.0%), and 3-mercaptopropionic acid (MPA, 99%) were purchased from Sigma-Aldrich, Korea, and 1-ethyl-3-(3-dimethylaminopropyl)carbodiimide (EDC, 98%), and *N*-hydroxysulfosuccinimide (sulfo-NHS, 98%) were purchased from Tokyo Chemical Industry, Japan. High purity deionized water (18.2 MΩ cm^{-1}) was used in all of the procedures.

Isolation of PSI: The PSI protein was isolated by the established method with minor modifications.[26] Spinach (*Spinacia oleracea* L.) was purchased from a local market. 200 g of green spinach leaves was ground using a blender with 600 mL of washing buffer (0.3 M sucrose, 30×10^{-3} M Tris-HCl, 15×10^{-3} M NaCl, and pH 7.8) for 30 s. The obtained homogenate was filtered through two layers of Miracloth (with a pore size of 22–25 μm, CalBiochem) and centrifuged at 2000 g for 7 min. The light green supernatant was discarded, and the pallet was resuspended in a hypotonic buffer (5×10^{-3} M EDTA, 5×10^{-3} M Tris-HCl, and pH 7.8). The solution was sonicated for 2 min and centrifuged at 10 000 g for 15 min. The pallet was adjusted to 2.5 mg Chl L^1 using a basic buffer (0.3 M sucrose, 30×10^{-3} M Tris-HCl, pH 7.8) and 1.7% triton X-100 (w/v) was added. After gentle stirring for 30 min in the dark at 4 °C, the solution was centrifuged at 35 000 g for 30 min, and the supernatant was collected. The solution was adjusted to 2.0 mg Chl mL^{-1} using a basic buffer, and dodecyl-β-D-maltoside (DDM) was added to produce a final concentration of 2.0% (w/v). After gentle stirring for 20 min in the dark at 4 °C, 9 mL of the solution was loaded onto a 24 mL 0.1–1.0 M sucrose gradient (containing the basic buffer and 0.05% DDM) with a 5 mL cushion of 2 M sucrose. After ultracentrifugation at 26 800 rpm for 17 h in a SW-32 rotor (Beckman), the lowest dark green band was collected with a syringe and frozen at –80 °C using 20% glycerol (v/v).

Characterization of PSI: The protein concentration was adjusted via the chlorophyll concentration. The chlorophyll concentration was determined after extraction in 80% acetone using a method that was developed by Arnon.[38] The proteins were analyzed using SDS-PAGE and a Coomassie blue staining step. The SDS-PAGE was carried out using 15% acrylamide resolving gels. Briefly, 10 μL of the samples and prestained protein size markers were loaded onto each well, and electrophoresis was performed at 100 V for 100 min. After the electrophoresis step, the gel was washed in distilled water for 10 min and rinsed with a fixation solution (containing 30% methanol and 10% acetic acid) for 30 min. After fixation, EzWayTM Protein-Quick Blue solution (Koma Biotech) was added and stained for 2 h.

Platinization of PSI: The extracted PSI was dialyzed in a 20×10^{-3} M sodium phosphate buffer with a pH of 7.2 (reaction buffer) for 24 h before platinization. The PtPSI was prepared by photodeposition using 30×10^{-3} M Asc and 0.2×10^{-3} M Dc as a sacrificial electron donor. The reaction proceeded in the reaction buffer with 0.05 mg Chl mL^{-1} PSI, 0.4×10^{-3} M $Na_2[PtCl_6]$ and an Asc/Dc couple (for a total volume of 10 mL). A continuous white LED bulb light illuminated the sample under vigorous stirring for 20 h. The PtPSI was washed with the reaction buffer before linking with the oxidation component to remove the remaining $Na_2[PtCl_6]$ and Asc/Dc.

Synthesis of $BiVO_4$: The hydrothermal method was used as previously reported.[31] Typically, 36.0 mmol of NH_4VO_3 (99%) and 36.0 mmol of $Bi(NO_3)_3{\cdot}5H_2O$ (98%) were dissolved in 220 and 80 mL of 2.0 M nitric acid solutions, respectively. The two solutions were mixed, and a yellow homogeneous solution was formed under stirring. The pH value of the solution was then adjusted to 2.0 using an ammonia solution under vigorous stirring until an orange precipitate was obtained. After further stirring for 0.5 h, the precipitate was aged for 2 h, and 70 mL of the subsided precipitate was transferred to a Teflon-lined stainless steel autoclave (100 mL) and hydrothermally heated to 473 K, which was held for 24 h. The resulting yellow powder was filtered following natural cooling to room temperature and dried in air at 60 °C.

Photodeposition of Metal on BiVO4: The metals (Au and Ag) were photodeposited onto the as-synthesized $BiVO_4$. $HAuCl_4$ and $AgNO_3$ were used as precursors for the Au and Ag deposition. Generally, 0.2 g of the as-synthesized $BiVO_4$ and 10 wt% of the metal precursor (by calculation) were stirred together in 100 mL of deionized water under irradiation by a 300-W Xe lamp (420-nm cut) for 3 h. The metal-deposited $BiVO_4$ (mt-$BiVO_4$) was washed with deionized water 3 times to remove the unreacted metal precursor before further chemical treatment and SEM analysis.

EDC/Sulfo-NHS Coupling: Finally, covalent linking between PtPSI and mt-$BiVO_4$ was carried out via EDC/sulfo-NHS coupling. First, 0.1 g of mt-BiVO4 was immersed in ethanolic 10×10^{-3} M MPA to carboxylate the metal particles. After gently stirring the solution for 24 h, the MPA-treated mt-$BiVO_4$ was rinsed with deionized water and finally diluted in 5 mL of 10×10^{-3} M MES buffer (pH 5.5). Then, 30 mg of EDC and 30 mg of sulfo-NHS were added, stirred for 2 h, and washed with the reaction buffer. Finally, l mL of 0.5 mg Chl mL^{-1} of the prepared PtPSI was added to the total solution volume and gently stirred for 24 h. The all-linked samples were washed twice with the reaction buffer to remove unlinked proteins. For reference, we added 1 mL of 0.5 mg Chl mL^{-1} of the PtPSI to 0.1 g of the carboxylated mt-$BiVO_4$ and stirred the resulting mixture for 24 h.

Characterization of Optical Properties: The irradiance of the light source was measured using a spectrum analyzer (International Light Technologies, ILT950). The UV–vis absorption spectra were measured using a NanoDropTM 2000c and a spectroscopic cuvette. The samples were dispersed in the reaction buffer, which was then place in a 1 mL cuvette for analysis. The UV–vis reflectance spectra were obtained using a UV-vis-NIR spectrometer (Agilent Technologies, Cary 5000).

Field Emission Scanning Electron Microscopy: The FESEM micrographs were obtained using a Zeiss, SUPRA 55VP operating at 2 kV. The FESEM samples were prepared by dropping the sample containing solutions onto silicon wafers and drying in air.

X-Ray Powder Diffraction: The phase composition of the synthesized powder was determined using X-ray powder diffraction (XRD, Bruker, AXS D8 Advance) with CuKα radiation. The XRD patterns were recorded in a 2θ range of 10°–60°. The step size and the counting time were 0.02° and 0.25 s, respectively. The XRD patterns were analyzed using an EVA software package (Bruker AXS) to identify the phases present.

Photoluminescence: The PL spectra were taken using a PTI QuantaMasterTM spectrofluorometer, QM4 (Photon Technology International, Birmingham, NJ) with an excitation wavelength of 340 nm, a scan range of 450–660 nm and a step size of 1 nm. Each sample was placed in a cuvette and stirred vigorously to disperse the particles. Typically, 1 mg of sample was put into 3 mL of the reaction buffer. When the mt-$BiVO_4$ was mixed or linked with PtPSI, the additional washing step for the removal of the unlinked protein was skipped.

Gas Chromatography: The quantitative detection of hydrogen was performed by gas chromatography (GC, PerkinElmer, NARL8502 Model 4003). Typically, 0.05 g of the PtPSI-mt-$BiVO_4$ in 20 mL of the reaction buffer was placed in a tightly capped vial and stirred vigorously during the photoreaction. 1 mL of the final gas was ejected into the gas chromatograph by a syringe at the designated time. The GC measured the molar proportion of the hydrogen gas relative to the total ejected gas, and the exact amount of gas was calculated by multiplying by the empty space in the vial reactor.

Acknowledgements

Y.K. and D.S. contributed equally to this work. This research was supported by the Basic Science Research Program (Grant No. 2011–0011225), the Global Frontier R&D Program on Center for

Multiscale Energy System (Grant No. 0420–20130104), and the Fusion Research Program for Green Technologies (Grant No. 2012M3C1A1048863) of the National Research Foundation of Korea (NRF) funded by the Ministry of Science, ICT & Future, Korea. This research was also supported by Research Institute of Advanced Materials (RIAM) at Seoul National University. Y.K. is grateful to the Global PH.D Fellowship Program through the National Research Foundation of Korea (NRF) funded by the Ministry of Education (Grant No. 2013034602).

Received: December 24, 2014
Revised: February 2, 2015
Published online: February 18, 2015

[1] a) K. Brettel, W. Leibl, *Biochim. Biophys. Acta, Bioenerg.* **2001**, *1507*, 100; b) K. Brettel, *Biochim. Biophys. Acta, Bioenerg.* **1997**, *1318*, 322.
[2] D. O. Hall, K. Rao, *Photosynthesis*, Cambridge University Press, Cambridge, Cambridgeshire, UK **1999**.
[3] A. J. Bard, *J. Photochem.* **1979**, *10*, 59.
[4] Y. Sasaki, H. Kato, A. Kudo, *J. Am. Chem. Soc.* **2013**, *135*, 5441.
[5] H. Kato, Y. Sasaki, N. Shirakura, A. Kudo, *J. Mater. Chem. A* **2013**, *1*, 12327.
[6] J. Qi, K. Zhao, G. Li, Y. Gao, H. Zhao, R. Yu, Z. Tang, *Nanoscale* **2014**, *6*, 4072.
[7] K. Maeda, M. Higashi, D. Lu, R. Abe, K. Domen, *J. Am. Chem. Soc.* **2010**, *132*, 5858.
[8] K. Maeda, N. Saito, D. Lu, Y. Inoue, K. Domen, *J. Phys. Chem. C* **2007**, *111*, 4749.
[9] J. Ran, J. Zhang, J. Yu, S. Z. Qiao, *ChemSusChem* **2014**, *7*, 3426.
[10] J. Ran, J. Zhang, J. Yu, M. Jaroniec, S. Z. Qiao, *Chem. Soc. Rev.* **2014**, *43*, 7787.
[11] A. Iwase, Y. H. Ng, Y. Ishiguro, A. Kudo, R. Amal, *J. Am. Chem. Soc.* **2011**, *133*, 11054.
[12] H. J. Yun, H. Lee, N. D. Kim, D. M. Lee, S. Yu, J. Yi, *ACS Nano* **2011**, *5*, 4084.
[13] a) Maeda, K. Teramura, D. Lu, T. Takata, N. Saito, Y. Inoue, K. Domen, *Nature* **2006**, *440*, 295; b) Y. Lee, H. Terashima, Y. Shimodaira, K. Teramura, M. Hara, H. Kobayashi, K. Domen, M. Yashima, *J. Phys. Chem. C* **2007**, *111*, 1042.
[14] I. J. Iwuchukwu, M. Vaughn, N. Myers, H. O'Neill, P. Frymier, B. D. Bruce, *Nat. Nanotechnol.* **2010**, *5*, 73.
[15] J. F. Millsaps, B. D. Bruce, J. W. Lee, E. Greenbaum, *Photochem. Photobiol.* **2001**, *73*, 630.
[16] B. R. Evans, H. M. O'Neill, S. A. Hutchens, B. D. Bruce, E. Greenbaum, *Nano. Lett.* **2004**, *4*, 1815.
[17] a) R. A. Grimme, C. E. Lubner, D. A. Bryant, J. H. Golbeck, *J. Am. Chem. Soc.* **2008**, *130*, 6308; b) R. A. Grimme, C. E. Lubner, J. H. Golbeck, *Dalton Trans.* **2009**, *45*, 10106.
[18] a) M. Ihara, H. Nishihara, K. S. Yoon, O. Lenz, B. Friedrich, H. Nakamoto, K. Kojima, D. Honma, T. Kamachi, I. Okura, *Photochem. Photobiol.* **2006**, *82*, 676; b) M. Ihara, H. Nakamoto, T. Kamachi, I. Okura, M. Maedal, *Photochem. Photobiol.* **2006**, *82*, 1677; c) H. Krassen, A. Schwarze, B. Friedrich, K. Ataka, O. Lenz, J. Heberle, *ACS Nano* **2009**, *3*, 4055; d) C. E. Lubner, P. Knorzer, P. J. N. Silva, K. A. Vincent, T. Happe, D. A. Bryant, J. H. Golbeck, *Biochemistry* **2010**, *49*, 10264; e) C. E. Lubner, A. M. Applegate, P. Knörzer, A. Ganago, D. A. Bryant, T. Happe, J. H. Golbeck, *Proc. Natl. Acad. Sci. U.S.A.* **2011**, *108*, 20988.
[19] S. C. Silver, J. Niklas, P. Du, O. G. Poluektov, D. M. Tiede, L. M. Utschig, *J. Am. Chem. Soc.* **2013**, *135*, 13246.
[20] L. M. Utschig, S. C. Silver, K. L. Mulfort, D. M. Tiede, *J. Am. Chem. Soc.* **2011**, *133*, 16334.
[21] P. Zhou, J. Yu, M. Jaroniec, *Adv. Mater.* **2014**, *26*, 4920.
[22] a) Z. B. Yu, Y. P. Xie, G. Liu, G. Q. Lu, X. L. Ma, H. M. Cheng, *J. Mater. Chem. A* **2013**, *1*, 2773; b) H. Tada, T. Mitsui, T. Kiyonaga, T. Akita, K. Tanaka, *Nat. Mater.* **2006**, *5*, 782; c) X. Wang, G. Liu, L. Wang, Z. G. Chen, G. Q. Lu, H. M. Cheng, *Adv. Energy Mater.* **2012**, *2*, 42.
[23] M. L. Guan, D. K. Ma, S. W. Hu, Y. J. Chen, S. M. Huang, *Inorg. Chem.* **2011**, *50*, 800.
[24] X. Zhang, Y. L. Chen, R. Liu, D. P. Tsai, *Rep. Prog. Phys.* **2013**, *76*, 046401.
[25] A. Nakamura, T. Suzawa, Y. Kato, T. Watanabe, *FEBS Lett.* **2005**, *579*, 2273.
[26] X. Qin, K. Wang, X. Chen, Y. Qu, L. Li, T. Kuang, *Photosynth. Res.* **2006**, *90*, 195.
[27] Y. Suemori, M. Nagata, Y. Nakamura, K. Nakagawa, A. Okuda, J. Inagaki, K. Shinohara, M. Ogawa, K. Iida, T. Dewa, K. Yamashita, A. Gardiner, R. J. Cogdell, M. Nango, *Photosynth. Res.* **2006**, *90*, 17.
[28] R. G. Li, F. X. Zhang, D. G. Wang, J. X. Yang, M. R. Li, J. Zhu, X. Zhou, H. X. Han, C. Li, *Nat. Commun.* **2013**, *4*, 1432.
[29] A. Kudo, K. Omori, H. Kato, *J. Am. Chem. Soc.* **1999**, *121*, 11459.
[30] C. Li, P. Zhang, R. Lv, J. Lu, T. Wang, S. Wang, H. Wang, J. Gong, *Small* **2013**, *9*, 3950.
[31] D. Wang, R. Li, J. Zhu, J. Shi, J. Han, X. Zong, C. Li, *J. Phys. Chem. C* **2012**, *116*, 5082.
[32] A. B. Shem, F. Frolow, N. Nelson, *Nature* **2003**, *426*, 630.
[33] J. R. Fernández, J. P. Juste, F. J. G. de Abajo, L. M. L. Marzán, *Langmuir* **2006**, *22*, 7007.
[34] H. Liang, W. Wang, Y. Huang, S. Zhang, H. Wei, H. Xu, *J. Phys. Chem. C* **2010**, *114*, 7427.
[35] a) X. Wang, S. Li, Y. Ma, H. Yu, J. Yu, *J. Phys. Chem. C* **2011**, *115*, 14648; b) J. Hou, Z. Wang, C. Yang, W. Zhou, S. Jiao, H. Zhu, *J. Phys. Chem. C* **2013**, *117*, 5132; c) L. Ye, J. Liu, C. Gong, L. Tian, T. Peng, L. Zan, *ACS Catal.* **2012**, *2*, 1677.
[36] X. Ma, K. Zhao, H. Tang, Y. Chen, C. Lu, W. Liu, Y. Gao, H. Zhao, Z. Tang, *Small* **2014**, *10*, 4664.
[37] a) L. Ge, *Mater. Chem. Phys.* **2008**, *107*, 465; b) S. Kohtani, K. Yoshida, T. Maekawa, A. Iwase, A. Kudo, H. Miyabe, R. Nakagaki, *Phys. Chem. Chem. Phys.* **2008**, *10*, 2986.
[38] D. I. Arnon, *Plant Physiol.* **1949**, *24*, 1.